

# Potential Gastric Cancer Immunotherapy: Stimulating the Immune System with *Helicobacter pylori* pIRES2-DsRed-Express-ureF DNA Vaccines

Mahsa Afkhamipour<sup>1</sup> · Fatemeh Kaviani<sup>1</sup> · Samaneh Dalali<sup>1</sup> · Tohid Piri-Gharaghie<sup>1,2</sup> · Abbas Doosti<sup>1</sup>✉

## Abstract

Most gastric cancers (GC) are thought to be caused by *Helicobacter pylori* (*H. pylori*) infections. However, there is mounting evidence that GC patients with positive *H. pylori* status have improved prognoses. The *H. pylori*-induced cellular immune reaction may inhibit cancer. In this study, BALB/c mice were immunized using recombinant plasmids that encode the *ureF* gene of *H. pylori*. Purified functional splenic CD3<sup>+</sup> T lymphocytes are used to study the anticancer effects *in vitro* and *in vivo*. The immunological state of GC patients with ongoing *H. pylori* infection is mimicked by the *H. pylori* DNA vaccines, which cause a change in the reaction from Th1 to Th2. Human GC cells grow more slowly when stimulated CD3<sup>+</sup> T lymphocytes are used as adoptive infusions because they reduce GC xenograft development *in vivo*. The more excellent ratios of infiltrating CD8<sup>+</sup>/CD4<sup>+</sup> T cells, the decreased invasion of regulatory FOXP3<sup>+</sup> Treg lymphocytes, and the increased apoptosis brought on by Caspase9/Caspase-3 overexpression and Survivin downregulation may all contribute to the consequences. Our findings suggest that in people with advanced GC, *H. pylori* pIRES2-DsRed-Express-ureF DNA vaccines may have immunotherapeutic utility.

## Keywords

Gastric carcinoma · *Helicobacter pylori* · DNA vaccine · *ureF* gene

Received: 26 February 2023 / Accepted: 20 September 2023/  
© L. Hirszfeld Institute of Immunology and Experimental Therapy, Wrocław, Poland 2023

## 1. Introduction

Gastric adenocarcinoma is the second most prevalent cancer-related cause of death globally, coming in at number four after lung, breast, and colorectal cancers, particularly in low- and middle-income nations like Asia (Ranjbar and Chehelgerdi 2018). morbidity and death rates are caused by gastric cancer (GC), and *Helicobacter pylori* (*H. pylori*) infection, a category one carcinogen according to the National Agency for Research on Cancer, is responsible for >80% of the global GC burden. The *H. pylori* strain strongly correlates with intestinal metaplasia and GC prevalence. The bacteria *H. pylori*, which lives in the stomach, causes chronic gastritis, the primary cause of most cases of GC (Chehelgerdi and Doosti 2020). Approximately, half of humanity is affected by the bacterium, a flagellar microaerophilic Gram-negative bacillus (O'Connor et al. 2020). In Western nations, the frequency of infections ranges 10–60%, but in underdeveloped nations, it can reach up to 90% during maturity (Mezmale et al. 2020).

In addition, research has revealed that the most common way that *H. pylori* infections are spread is from mother to child. This is especially true for young children under 5 years

(Fakharian et al. 2022). *H. pylori* can colonize and remain in a particular biological niche inside the gastric lumen, where it may live in the acidic conditions of the stomach (Zhang et al. 2022). The helical structure of this human infection causes the bacteria to enter and stay in the stomach lining, behind the mucus, and it manages to evade the host immune system's defenses (Kusters et al. 2006; Tilahun et al. 2022). According to several lines of evidence, *H. pylori* infections are linked to the etiology of chronic proximal gastroenteritis, chronic gastritis, and GC (Malfertheiner et al. 2022; Tempera et al. 2022). However, a combination of proton pump inhibitors and various antibiotic treatments is typically used to treat *H. pylori* pathogens. The rapid spread of antibiotic-resistant isolates and some observed side effects necessitate substituting such an expensive treatment with a different therapeutic strategy (Nagaraja and Eslick 2014). The majority of the *H. pylori*-associated pathogenicity factors have been identified, making the development of vaccines a potential strategy (Sharndama and Mba 2022).

Vaccines not only offer long-lasting defense, but also lessen the harmful effects of widespread antibiotic use on strains of *H. pylori* that are good for human health (Malfertheiner et al. 2022). However, *H. pylori* infection and serious problems can still occur in patients receiving pharmacological therapy for symptoms and those who are asymptomatic, and vaccinations may be able to solve this issue (Shatila and Thomas 2022). There have been significant efforts in recent years

<sup>1</sup> Biotechnology Research Center, Shahrekord Branch, Islamic Azad University, Shahrekord, Iran

<sup>2</sup> Biotechnology Research Center, East Tehran Branch, Islamic Azad University, Tehran, Iran

✉ doostiabbas2021@gmail.com

to increase the number of *H. pylori* vaccines based on the organism's essential virulence factors, such as the flagellum receptors, vacuolating enterotoxin, cytotoxin-associated antigen, urease, the pathogenic organisms island, and neutrophil-activating protein, whether in their native or recombinant configurations. Although the associated processes remain unexplained, these methods protect the laboratory mouse model (Maleki Kakelar et al. 2019). Nowadays, possible *H. pylori* antigens encoded via vector-based vaccines have also been considered; however, the methods mentioned above have yet to shield the host from infection (Park et al. 2022). Since DNA vaccines are generally safe and stable and generate cellular and humoral immunity, researchers have recently focused more on vector-based vaccinations than recombinant protein vaccines. Additionally, incorporating DNA encoding the pathogen's antigen onto a bacterial plasmid may create these vaccines just as simply as polyvalent vaccinations (Maleki Kakelar et al. 2019). In this method, discovering the optimal vaccine against this prevalent human infection might arise from targeting conserved and essential genes of *H. pylori* to introduce in the vector (Kang et al. 2012; Xue et al. 2019). Studies now indicate that urease is a crucial element in the colonization of *H. pylori* in the host and the development of severe infection (Gupta et al. 2019). *Urease* is a potent immunogen that triggers a robust immune response and is essential for *H. pylori* metabolism and virulence. It is also required for the colonization of the gastric mucosa. This enzyme is a potential vaccine candidate for diagnosis, follow-up after therapy, and taxonomic identification. An intriguing paradigm for metallo-enzyme investigations is urease (Kafarski and Talma 2018). Prior to the identification of *H. pylori*, it was believed that humans produced "gastric urease." It is now understood that this bacteria, which inhabits the human stomach mucosa, is the source of this noteworthy protein. According to the previous papers, the current study's objectives were cloning and developing the *H. pylori*-derived urease gene encoding into the eukaryotic expression vector and assessing the immunomodulatory activity of such a recombinant construct in an animal model.

## 2. Materials and Methods

### 2.1. Vectors, cell lines, and animals

Invitrogen produced the pIRES2-DsRed-Express plasmid (Carlsbad, CA, USA). The human GC cell lines MKN28 and AGS, as well as the HEK 293-T cells, were bought from the Iranian Biological Resource Center (Iran) and cultured in DMEM (Hyclone, Logan, UT, USA) with 10% fetal bovine serum, 100 U/mL penicillin, and 100 mg/mL streptomycin (Sigma-Aldrich, USA). Female BALB/c mice that were 6 weeks old and normal and nude (nu/nu) were acquired from the Biotechnology Research Center of Islamic Azad

University, Shahrekord branch (Shahrekord, Iran) and kept under specified pathogen-free conditions. The Biotechnology Research Center of Shahrekord Islamic Azad University's Ethics Committee's instructions for the correct use and care of laboratory animals were followed when conducting the animal research.

### 2.2. Construction of *H. pylori* DNA vaccines

The BGI Genomics Company produced the *ureF* gene independently (Shenzhen, China). The *ureF* gene was subsequently inserted into the plasmids pIRES2-DsRed-Express (Invitrogen, USA) to generate pIRES2-DsRed-Express-*ureF*, which was verified by DNA sequencing and endonuclease digestion assays using *Bam*HI (GGATCC) and *Eco*RV (GATATC). The constructs have 20 repeats of the CpG ODN C274 motif (5'-TCGTCGAACGTTTCGAGATGAT-3') and a Kozak nucleotide at the N-terminus to boost immunological response. Lipofectamine 2000 was used to transiently transfect the generated plasmids into HEK 293-T cells to confirm the eukaryotic expression vector (Invitrogen). After 48 h of transfection, the cells were collected and lysed. The total cellular proteins were then analyzed using a Western blot kit and a rabbit anti-*H. pylori* polyclonal antibody (pAb) from LifeSpan BioSciences in Seattle, Washington, USA, following the manufacturer's instructions.

### 2.3. Immunization of mice by DNA vaccines

Randomly selected BALB/c mouse groups (Table S1 in Supplementary Material) received a DNA immunization (100 µg of plasmid) and an injection of the immunogen combination into the double hind thigh (0.3 mL per mouse). For three rounds, 0.3 mL of orbital blood was obtained from each of the animals (five per group), who had immunizations at days 0, 15, and 30. The empty vector served as the vehicle control, and orbit blood tests were also collected 2 weeks after the most recent vaccine. To make the single-cell suspensions, the animals' spleens were removed after cervical dislocation sacrifice. Before separating and transferring the splenic T cells, the related immunological response was first ascertained using the splenic cells and blood samples.

### 2.4. Enzyme-linked immunosorbent assay (ELISA)

The appropriate Mouse ELISA Quantitation Kit (Montgomery, USA) was used to measure the levels of IgG1 and IgG2a in the serum of vaccinated mice. Using mouse Quick ELISA kits, the quantities of interleukin (IL)-4, IL-17, interferon (IFN)-γ, and tumor necrosis factor (TNF)-α were measured using the double-antibody sandwich ELISA technique (Dakewe Biotech, China). Following the manufacturers' suggested practices, each test was run twice.

## 2.5. Real-time PCR assay

The spleen and small intestine of the mice were removed under aseptic conditions and kept in liquid nitrogen at  $-198^{\circ}\text{C}$ . Then, tissues were processed using the YTA kits' instructions for RNA extraction and cDNA synthesis (Yekta Tajhiz, Iran). The *GAPDH* gene was utilized as an internal control during real-time PCR using the YTA SYBR Green master mix (Yekta Tajhiz, Iran). For real-time PCR, a reaction volume of 15  $\mu\text{L}$ , composed of 0.5  $\mu\text{L}$  cDNA, 0.5  $\mu\text{L}$  forward primer, 0.5  $\mu\text{L}$  reverse primer, 10  $\mu\text{L}$  master mix, and 3.5  $\mu\text{L}$  of double sterile distillation water, was employed. Primers are listed in Table 1. Along with initial denaturation for 10 min, the temperature cycle program also included 40 cycles at  $95^{\circ}\text{C}$  for 20 sec, annealing at  $53^{\circ}\text{C}$  for 1 min, and elongation at  $72^{\circ}\text{C}$  for 1 min, followed by the final elongation at  $72^{\circ}\text{C}$  for 10 min. The relative gene expression of IFN- $\gamma$ , TNF- $\alpha$ , IL-17, and IL-4 were calculated by using the  $2^{-\Delta\Delta\text{CT}}$  method and normalized to GAPDH levels in each sample.

## 2.6. Flow cytometry

The peripheral T-cell subpopulations were identified using flow cytometry in blood samples collected from each group's immunized animals. Red blood cell (RBC) lysis was performed on 100  $\mu\text{L}$  of fresh total blood under anticoagulation in 1 $\times$  RBC Lysis Solution (eBioscience, USA). Following the manufacturer's instructions, the company's CD3e PE-Cy5, CD4 PE, and CD8a FITC antibody cocktail were used to stain the cell surface. The cells were cleaned before being examined using FlowJo 7.6.5 tools and an LSRII flow cytometer from BD Pharmingen in San Diego, California (Tree Star, USA).

## 2.7. Purification of splenic CD3<sup>+</sup> pan-T cells

Following the removal of the spleens from the vaccinated mice, single spleen cell suspensions were generated. Following the suggested methods, the MiniMACSTM

Separator and Pan T Cell Purification Kit II (Miltenyi Biotec, USA) were utilized. By eliminating non-T cells such as B cells, natural killer (NK) cells, dendritic cells, macrophages, granulocytes, endothelium, and erythroid cells, pure CD3<sup>+</sup> pan-T cells were generated. The extracted CD3<sup>+</sup> T cells were submitted to flow cytometry using a combination of CD3e PE-Cy5, CD4 PE, and CD8a FITC antibodies from eBioscience in San Diego, California, and analyzed using FlowJo 7.6.5 software from Tree Star in the United States.

## 2.8. Cell viability assay

MTT analysis (Sangon Biotech, China) was used following the manufacturer's instructions to evaluate the *in vitro* anti-cancer activity of *H. pylori* vaccine-activated CD3<sup>+</sup> T cells. The effector cells were cocultured in 96-well plates with MKN28 and AGS cells for 24 h at a ratio of 1:25. The negative control was created using the splenic CD3<sup>+</sup> T cells from the mice who had received the vehicle immunization. The following formula was utilized to determine the inhibitory efficiency of effector cells:

$$\text{Inhibitory rate (\%)} = \left[ \frac{(1 - \text{optimum A of experimental group})}{\text{optimum A of control}} \right] \times 100\%.$$

Three duplicates of each experiment were run.

## 2.9. Analyze the colony growth and proliferation of CCK-8

With the aid of a CCK-8 detection kit, the CCK-8 assessment was completed (Dojindo Japan). Before the cell lines received the CCK-8 chemical treatment, the transfected cells were seeded into culture plates and grown for 10 h. 450 nm was used to measure absorbance.

## 2.10. Transwell invasion screenings

Cancer cells were placed on a pre-coated plate with adherent cells in a 24-well transwell tube (Corning) (BD Biosciences, San Jose, CA, USA). After 24 h of treatment, the top surfaces were brushed, and the invaded regions were fixed with 4% paraformaldehyde and stained with Giemsa. Afterward, the optical microscope was used to observe the cells.

## 2.11. In vivo anticancer efficacy evaluation

The *H. pylori*-activated CD3<sup>+</sup> T cells were administered through adoptive transfusion to a nude BALB/c animal model with GC xenograft. Briefly,  $1 \times 10^7$  MKN28 cells were injected into the right forelimb armpit of female mice 6 weeks old. Every 3 days for three rounds,  $2 \times 10^7$  CD3<sup>+</sup> T cells were infused into the caudal vein after the subcutaneous cancer nodules reached a size of roughly 100 mm<sup>3</sup>. Every 2 days, the tumor volume (V) was measured using calipers and

**Table 1.** Sequence of specific primers for real-time PCR reaction

Gene	Size	Primer sequence
<i>IFN-<math>\gamma</math></i>	188 bp	F: 5'- GCCTAGCTCTGAGACAATGAACG -3' R: 5'- GCCAGTTCCTCCAGATATCCAAG -3'
<i>IL4</i>	263 bp	F: 5'- TCACAGGAGAAGGACGCCATG -3' R: 5'- TGGACTTGGACTCATTGATGGTGC -3'
<i>IL17</i>	246 bp	F: 5'- CTACAGTGAAGGCAGCAGCGATC -3' R: 5'- CTTTCCTCCGCATTGACACAG -3'
<i>GAPDH</i>	250 bp	F: 5'- ACCTTGGAATAAATGGGAAG -3' R: 5'- CTTCTGTGTGCTGTAGTTGC -3'
<i>ureF</i>	802 bp	F: 5'- GTTGATAAAAGTTCCTGGCT -3' R: 5'- ACATGCATCGAAATATGATGTGCA -3'

IFN, interferon; IL, interleukin.

computed using the formula:  $V = a b^2/2$ , where  $a$  and  $b$  stand for the main and minor axes of cancer, respectively. Two weeks following the last T-cell infusion, the mice were killed by cervical dislocation, and the cancer nodules were excised and employed in later research.

### 2.12. Immunohistochemistry (IHC)

The EnVision approach was used to use IHC to identify the subset of infiltrating immune cells in the tumor tissue sections. The segments were briefly cleaned with xylene, rehydrated with alcohol, and then cleaned once more with PBS. Anti-CD4 (Santa Cruz Biotechnology, USA), anti-CD8 (Santa Cruz, USA), anti-FOXP3 (Abgent, USA), anti-CD56 (Dako, USA), anti-CD68 (Dako, USA), anti-CD86 (Dako, USA), and anti-CD163 (Dako, USA) pAbs were incubated with the samples overnight at 4°C. After removing the main antibodies, Dako applied the Envision-plus detecting system's components. Hematoxylin was used as a counterstain, and an aqueous mounting media was used as a cover slip. Optical microscopy was used to evaluate the slides, and the positive index was derived using the ratio of stained cells.

### 2.13. Western blotting

Following adoptive transfusions of CD3<sup>+</sup> T cells, a Western blot analysis was done to identify apoptosis and antiapoptosis mechanisms in the GC xenograft. Following 12% SDS-PAGE separation and electrophoretically transfer to PVDF membranes, identical quantities of molecules from the tumor tissues were isolated. After the membranes had been blocked with 5% non-fat milk, individuals were probed with specific antibodies, including anti-Survivin rabbit polyclonal antibodies from Santa Cruz Biotechnology, anti-Caspase 9 mouse monoclonal antibodies from Cell Signaling Technology in Beverly, Massachusetts, and anti-Cleaved Caspase 3 mouse monoclonal antibodies (Cell Signaling Technology, 1:1000). The immunoreactive patterns were detected by enhanced chemiluminescence on the SuperSignal substrate platform (Rockford, USA) after the membranes had been washed and treated with HRP-conjugated goat anti-rabbit/mouse IgG (Cell Signaling Technology, 1:20,000).

### 2.14. Statistical analysis

Every study was conducted twice, and the data were presented as mean  $\pm$  SD. The group variations were examined using one-way ANOVA and independent variables  $t$ -tests. The analysis was done with SPSS software, and the graphics were made with Graph-Pad Prism. A  $P$ -value of  $<0.05$  was used to indicate significance.

## 3. Results

### 3.1. The DNA vaccine against *H. pylori* was constructed correctly

The *ureF* gene was inserted into the eukaryotic expression vector pIRES2-DsRed-Express to construct the DNA vaccine structure depicted in Figure S1 in Supplementary Material. The recombinant plasmid's genetic composition was used to measure the success of the cloning process. Moreover, DNA examination revealed that the virulence gene sequence of the recombinant plasmid was 100% similar to that of the *H. pylori* bacteria (Figure S2 in Supplementary Material). The generated plasmid was digested with *Bam*HI and *Eco*RV. Single colonies of transformed bacteria containing a plasmid with *ureF* gene are shown in Figure S3 in Supplementary Material. The effectiveness of the recombinant plasmid synthesis was shown by electrophoretic separation of the digestion fragments around 802 bp, encoding the *ureF* gene (Figures 1a and 1b). Blast was used to look over the recombinant plasmid sequencing outcomes. Recombinant plasmids with an E-value of  $8e-94$  and Per.Ident was 98.57%, similar to the target bacterium. The expression of target proteins encoded by relevant inserted genes is confirmed by Western blotting assay after the recombinant vector is reversibly transfected into HEK 293-T cells (Figure 1c). The plasmid vaccines containing the aforementioned *H. pylori ureF* gene fragments have thus been effectively created.

### 3.2. *H. pylori* DNA vaccines' induction of an immune response

The effectiveness and subtypes of the corresponding immune function are assessed after administering all recombinant *H. pylori* DNA vaccines to BALB/c mice. The concentrations of IL-4, IL-17, IFN- $\gamma$ , and TNF- $\alpha$  in the blood of vaccinated mice were also detected using the ELISA. The IgG1 and IgG2a concentrations noticeably increased by 1900 ng/mL to 3900 ng/mL and 4300 ng/mL to 6900 ng/mL, respectively, after the last vaccination in the vaccinated groups. IgG1/IgG2a ratio dropped from 2.26 to 1.76 fold after receiving *H. pylori* DNA vaccinations, showing that DNA vaccines were more effective at eliciting an IgG2a response (Figure 2a). In the pIRES2-DsRed-Express-*ureF* group, the levels of IL-4 and IFN- $\gamma$  in the blood dropped from 2800 ng/mL to 250 ng/mL and 3500 ng/mL to 980 ng/mL, respectively. The concentration of TNF- $\alpha$  and IL-17 in the pIRES2-DsRed-Express-*ureF* group increased significantly. So the concentration of TNF- $\alpha$  increased from 2500 ng/mL to 7870 ng/mL (three folds), and the concentration of IL-17 increased from 1800 ng/mL to 19,800 ng/mL (11 folds). However, there are no appreciable increases in IL-4 serum levels across all groups (Figure 2). The primary immune reaction subtype is probably



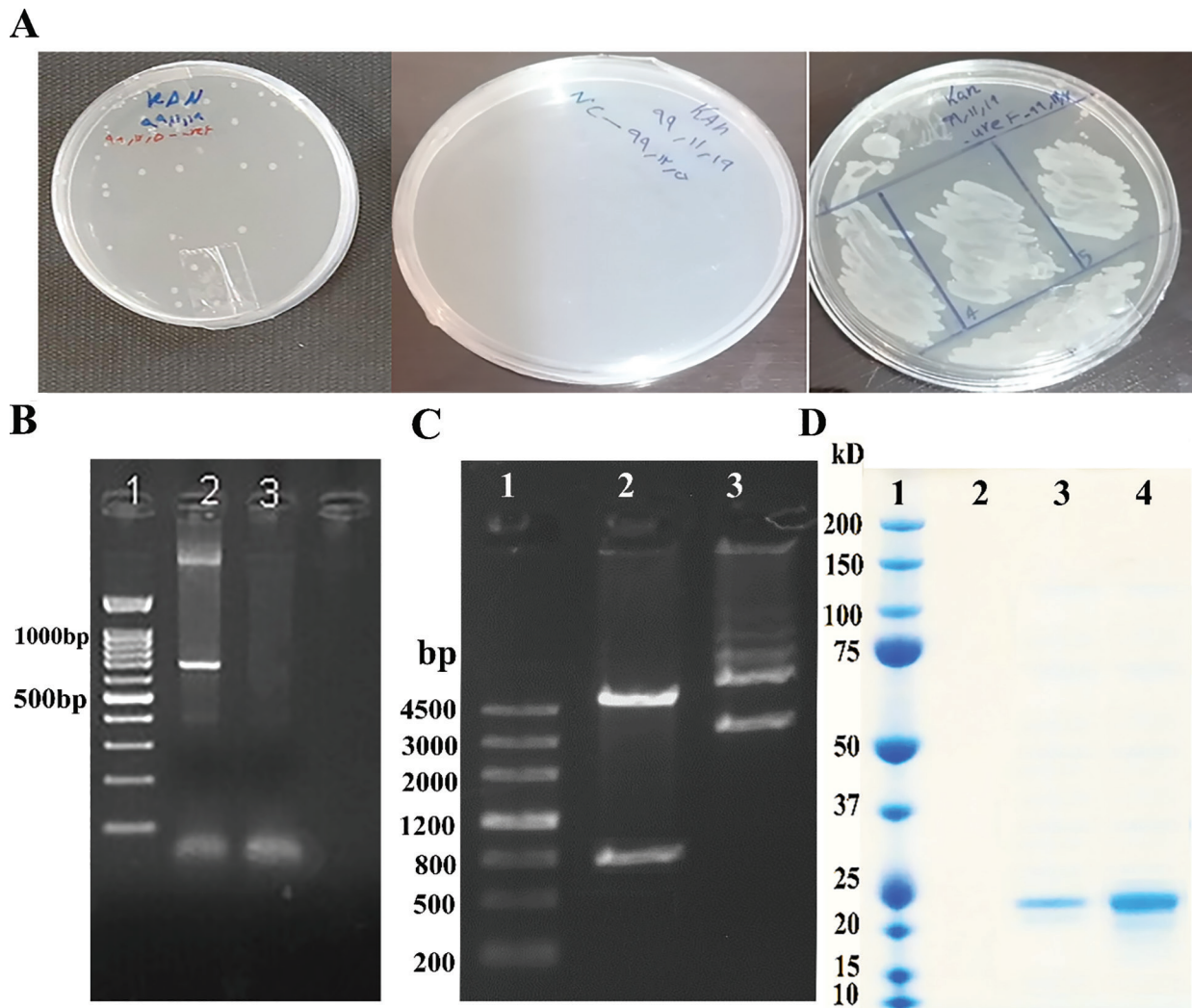


**Fig 1.** (A) Single colonies of transformed bacteria containing plasmid with *ureF* gene; Non-growth of vector-free cells in agar medium containing the antibiotic kanamycin (negative control); Preparation of matrix from a number of selected colonies. (B) Validation of 805 base pairs of *ureF* gene in *H. pylori* genome by PCR test, 1: DNA markerIII, 2: 805 base pairs of *ureF* gene, 3: Negative control; (C) the successful production of the recombinant plasmid. 1: DNA markerIII, 2: recombinant pIRES2-DsRed-Express-*ureF* before digestion, 3: recombinant pIRES2-DsRed-Express-*ureF* after digestion; (D) Expression of recombinant pIRES2-DsRed-Express-*ureF* in protein level. 1: Protein marker, 2: Negative control; 3 and 4: pIRES2-DsRed-Express-*ureF*.

a combined pattern of T helper (Th)1 and 2 cells, but with polarization to the Th2 profile after vaccination, according to the IgG1 and IgG2a reactions and dynamic changes in cytokine levels (Figure 2).

### 3.3. The transcription level of cytokines increased in the spleen and small intestine

The quantity of cytokine transcription in the spleen and small intestine was assessed using a quantitative real-time PCR technique. In the spleen of pIRES2-DsRed-Express-*ureF* vaccination groups, the IL-17 and TNF- $\alpha$  transcription levels were significantly higher than those in other groups (Figure 3a). Also, in small intestine tissue, real-time PCR

findings from the pIRES2-DsRed-Express-*ureF* vaccination groups showed significantly different levels of IL-17 and TNF- $\alpha$  gene expression from the other groups, and these results were also consistent with ELISA (Figure 3b). IL-4 and IFN- $\gamma$  transcription levels were not considerably different in the pIRES2-DsRed-Express-*ureF* group and other groups. After the final immunization, blood samples from the animals were obtained and submitted to flow cytometry to determine the peripheral T-cell subpopulations. The DNA vaccines, except for the pIRES2-DsRed-Express-*ureF* group, increase the proportions of CD3<sup>+</sup>, CD4<sup>+</sup>, and CD8<sup>+</sup> T-cell subgroups in the inoculated mice compared to the other group. As a result, the *H. pylori* DNA vaccine stimulates the Th cell response and changes the Th1 pro-inflammatory response into the Th2

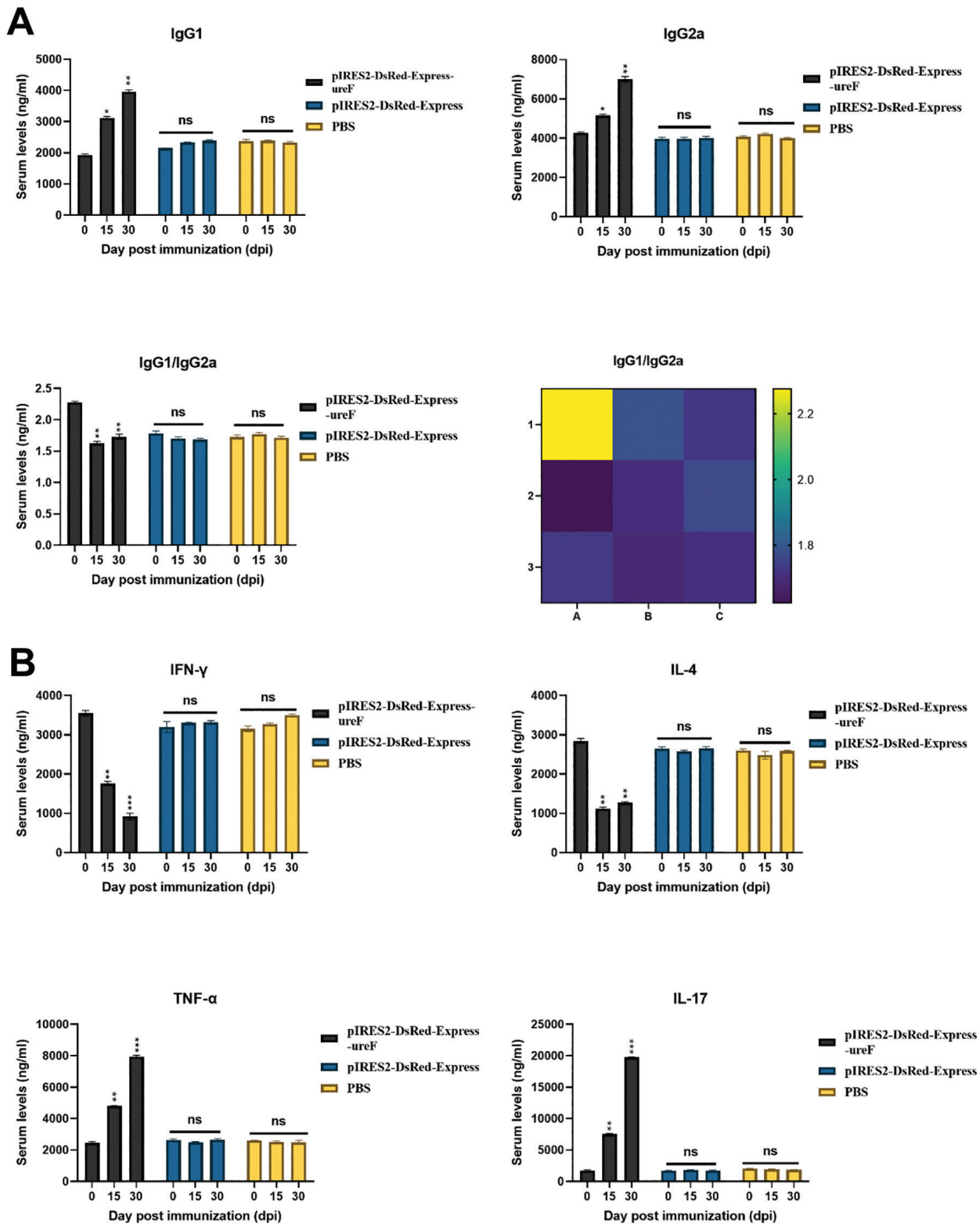


**Fig 2.** An analysis of the immunological responses and suppressive effects of splenic T-cells induced by *H. pylori* DNA immunizations. (A) ELISA measured serum IgG1 and IgG2a concentrations in several groups of vaccinated mice. (B) ELISA measurements of TNF- $\alpha$ , IFN- $\gamma$ , IL-4, and IL-17 relative levels and concentrations in different mouse immunization groups. \* $P < 0.05$ , \*\* $P < 0.01$ , \*\*\* $P < 0.001$  and ns: not significant.

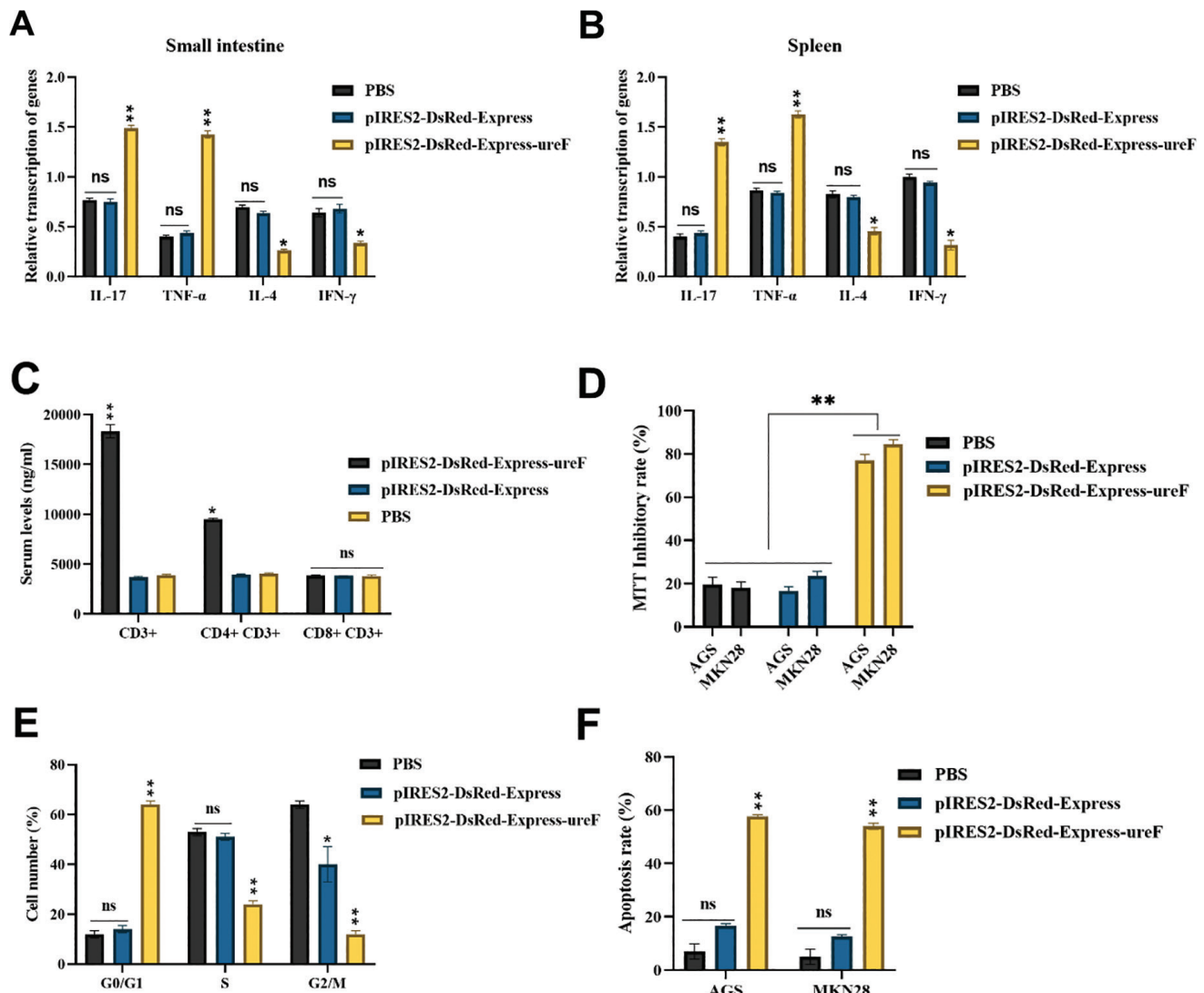


**Fig 3.** Cytokine levels were found in the small intestine (A) and spleen (B) of the control and immunized groups. (C) Peripheral CD3<sup>+</sup>, CD4<sup>+</sup>, and CD8<sup>+</sup> T-cell subpopulations in vaccinated mice were analyzed by flow cytometry. The immunization against pIRES2-DsRed-Express-ureF suppresses the invasion and growth of cancerous cells in the culture. (D) The MTT test examined the growth indices of three groups of AGS and MKN28 cells. Compared to the control group, the growth rate in the pIRES2-DsRed-Express-ureF group was considerably reduced. (E) Cell cycle regulation in cells was investigated using flow cytometry. Compared to the control group, the pIRES2-DsRed-Express-ureF vaccination group showed an increase in G0/G1 reduction in the proportion of the S phase to the G2/M phase. (F) The proportion of apoptotic cells was higher in the pIRES2-DsRed-Express-ureF vaccination group. \* $P < 0.05$ , \*\* $P < 0.01$ , and ns: not significant.

anti-inflammatory reaction. This imitates the immunological state of animals with chronic *H. pylori* infection while encouraging TNF- $\alpha$  production and T-cell proliferation (Figure 3c).

### 3.4. The pIRES2-DsRed-Express-ureF vaccine suppresses malignant cell proliferation and invasion

The impact of pIRES2-DsRed-Express-ureF vaccination on AGS and MKN28 cell proliferation was assessed using MTT. All pIRES2-DsRed-Express-ureF vaccine groups showed a substantial reduction in the growth rate of AGS and MKN28

cancer cells ( $P < 0.001$ ), and there was a significant variation between the growth percentages of the control and pIRES2-DsRed-Express-ureF vaccine groups (Figure 4a). An Annexin V-PI staining procedure was utilized to look at any differences in apoptosis between the experimental groups. Accelerated cell proliferation was related to cell cycle progression. Cell cycle control in the groups that had received vaccinations was investigated using flow cytometry. Compared to the control groups, pIRES2-DsRed-Express-ureF-vaccinated cells had higher G0/G1 and lowered S phase to G2.M phase ratios. These results showed that pIRES2-DsRed-Express-ureF



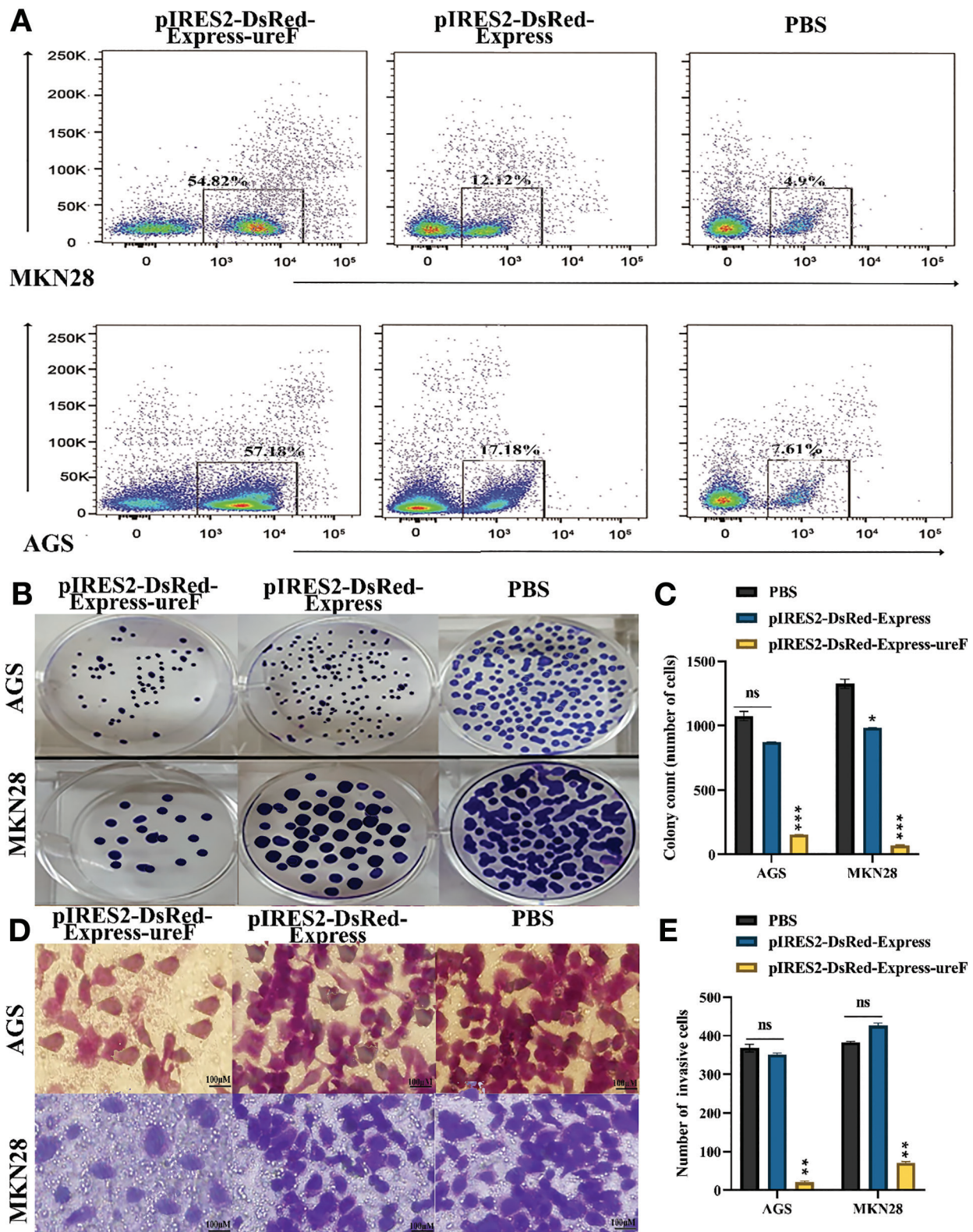


**Fig 4.** The immunization against pIRES2-DsRed-Express-ureF suppresses the invasion and growth of cancerous cells in the culture. (A) According to a flow cytometry experiment, pIRES2-DsRed-Express-ureF caused 54.82 and 57.18% of AGS and MKN28 cells to undergo apoptosis, respectively. (B,C) The colony formation assay using pIRES2-DsRed-Express-ureF transfected AGS and MKN28 cells revealed that they proliferated. (D,E) The quantity of invading AGS and MKN28 cells. \* $P < 0.05$ , \*\* $P < 0.01$ , \*\*\* $P < 0.001$  and ns, not significant.



vaccination prevented cell cycle progression (Figure 4b). The ratios of early, late, necrotic, and surviving cells are shown in Figures 4c and d. The percentage of necrosis, late apoptosis, and early apoptosis in the control cells was <10%. Over 90% of the rates in control groups had viable cells. In AGS cells, the apoptosis percentages for pIRES2-DsRed-Express-*ureF* and pIRES2-DsRed-Express were 57.18% and 17.18%, respectively. In MKN28 cells, pIRES2-DsRed-Express-*ureF* and pIRES2-DsRed-Express triggered 54.82% and 12.12% apoptosis (Figures 4c and d).

AGS and MKN28 cell proliferation was decreased by pIRES2-DsRed-Express-*ureF* vaccination, as shown by colony formation assay and CCK-8 test (Figures 4e and f). According to the transwell invasion test analysis, the pIRES2-DsRed-Express-*ureF* vaccination decreased the amount of invading AGS and MKN28 cells, while control groups had the opposite impact (Figures 4g and h). As a result, *in vitro* immunization using pIRES2-DsRed-Express-*ureF* prevented AGS and MKN28 malignant cells from proliferating and invading.

### 3.5. *In vitro* and *in vivo* anticancer effect of *H. pylori* pIRES2-DsRed-Express-*ureF* vaccine

Immunomagnetic beads were utilized to separate the *H. pylori* pIRES2-DsRed-Express-*ureF* vaccine from the inoculated mice. These effector cells were co-cultured with two different types of GC cells (the MKN28 and AGS cell lines) to confirm the *in vitro* anticancer impact. Since GC and *H. pylori* infection are closely related, different CD3<sup>+</sup> T lymphocytes were mixed in equal amounts. *In vitro* co-cultures of CD3<sup>+</sup> T cells of various compositions are performed with the MKN28 and AGS cell lines. Figure 5a shows that pIRES2-DsRed-Express-*ureF* immunotherapy groups had more potent inhibitory effects in both GC cell lines when compared to the control ( $P < 0.01$ ). The most considerable inhibitory effects on MKN28 ( $81.6 \pm 1.3\%$ ) and AGS ( $88.9 \pm 2.3\%$ ) cells are shown by the combined CD3<sup>+</sup> T cells from the target group. Additionally, the CD3<sup>+</sup> T cells from the pIRES2-DsRed-Express-*ureF* group significantly inhibit cancer growth in the two GC cell lines.

The BALB/c mice are transfused with adoptive CD3<sup>+</sup> T cells after being overburdened with GC cells. Compared to the PBS control, tumor growth is inhibited in the immunotherapy treatments with increased tumor necrosis and decreased tumor size and weight (Figure 5b). The mice' body weight did not differ considerably across the groups (Figure 6a). Early on day 9 following CD3<sup>+</sup> T-cell transfer, the tumor size changed, indicating the anti-GC impacts of the *H. pylori* vaccine-activated T cells. These effects persisted for at least another week (Figure 6b).

When compared to the control group, the tumor volume in the pIRES2-DsRed-Express-*ureF* group has significantly decreased (Figure 6c). According to the changes in tumor size at day 15, the average tumor suppression rates for the pIRES2-DsRed-Express-*ureF*, pIRES2-DsRed-Express, and PBS groups were 82.3%, 20.1%, 5.2%, and 35.8%, respectively (Figure 6d). The findings indicate that GC development *in vivo* may be successfully inhibited by adoptively transferred CD3<sup>+</sup> T cells stimulated by the *H. pylori* pIRES2-DsRed-Express-*ureF* DNA vaccine.

### 3.6. Subpopulation of immune cells infiltrating tumors after CD3<sup>+</sup> T-cell infusion

IHC was used to analyze the subtypes of infiltrated CD3<sup>+</sup>, CD4<sup>+</sup>, and CD8<sup>+</sup> T cells in the intramuscular xenograft of GC. The positive index and the tumor-infiltrating CD4<sup>+</sup> T-cell concentrations in all treatment groups reveal lower levels ( $P < 0.01$ ) (Figure 7a). However, adoptive infusions of the *H. pylori* DNA immunization CD3<sup>+</sup> T cells have little effect on the infiltration of CD8<sup>+</sup> T cells in the malignant tissues. In line with this, the ratios of infiltrating CD8<sup>+</sup>/CD4<sup>+</sup> T cells rise dramatically across the board for all immunotherapy groups (Figure 7b). Additionally, compared to the PBS control, labeling of the regulating FOXP3<sup>+</sup> T (Treg) lymphocytes in the pIRES2-DsRed-Express-*ureF* group is lower (Figures 7c and d). Notably, neither the proportions of infiltrating CD86<sup>+</sup> macrophages nor the infiltrations of CD68<sup>+</sup> macrophages (Figures 7c and d), CD86<sup>+</sup> M1 macrophages (Figures 7e and f), CD56<sup>+</sup> NK cells (Figures 7e and f), or CD68<sup>+</sup> macrophages, indicate significant alterations.

### 3.7. Apoptosis and anti-apoptosis mechanisms promoted by *H. pylori* pIRES2-DsRed-Express-*ureF* vaccine

Several essential signaling molecules that are strongly connected with the apoptosis and anti-apoptosis mechanisms in GC are identified by Western blotting to recognize further the molecular intermediaries implicated in the anticancer activity of adoptive immunotherapy using the *H. pylori* pIRES2-DsRed-Express-*ureF* vaccine. Comparatively, to the controls, Survivin is considerably down-regulated in all pIRES2-DsRed-Express-*ureF* groups. Caspase-9 and Caspase-3 were dramatically upregulated in the pIRES2-DsRed-Express-*ureF* group. Infusion of the *H. pylori* pIRES2-DsRed-Express-*ureF* DNA vaccine has no discernible effect on Caspase-8 expression (Figure 8), indicating that upregulation of Caspase-9/Caspase-3 and downregulation of Survivin following adoptive transfusions of the *H. pylori* pIRES2-DsRed-Express-*ureF* vaccine may improve cellular apoptosis.

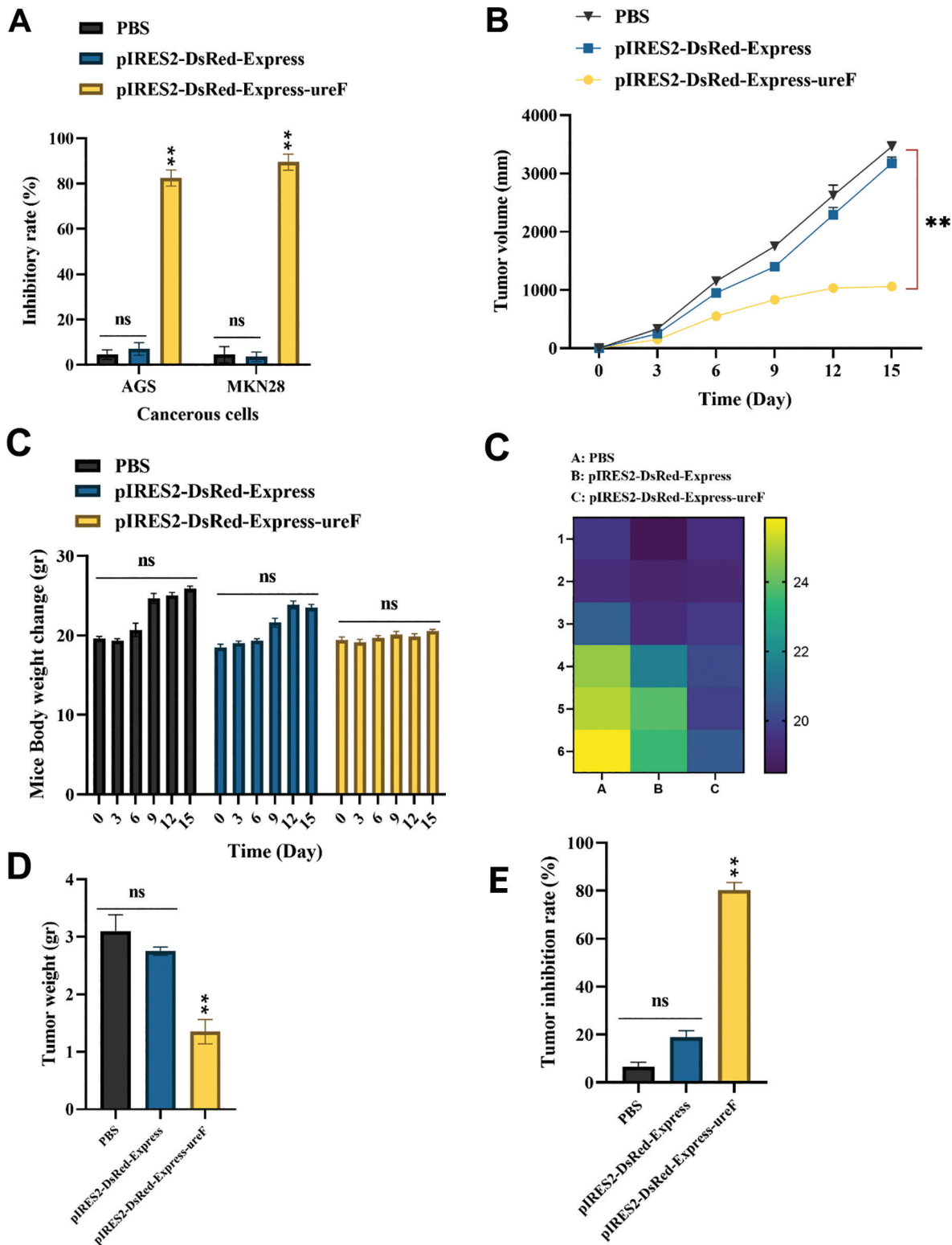


**Fig 5.** Splenic T-cells stimulated by *H. pylori* vaccinations have anticancer effects in vivo and in vitro. (A) The inhibition percentages of *H. pylori*-activated splenic T-cells on in vitro-cultured AGS and MKN28 cell lines. (B) Splenic T-cells stimulated by *H. pylori* vaccinations have anticancer effects in vivo. Mouse body weight variation curves from day 0 to day 15 after adoptive infusions. (C) Tumor nodule size curves in animals from 0 to 15 days following T-cell infusions. (D) The mean weights of the mouse tumor nodules that were excised. (E) The levels of tumor inhibition in the various experimental groups. \* $P < 0.05$ , \*\* $P < 0.01$ , and ns: not significant.

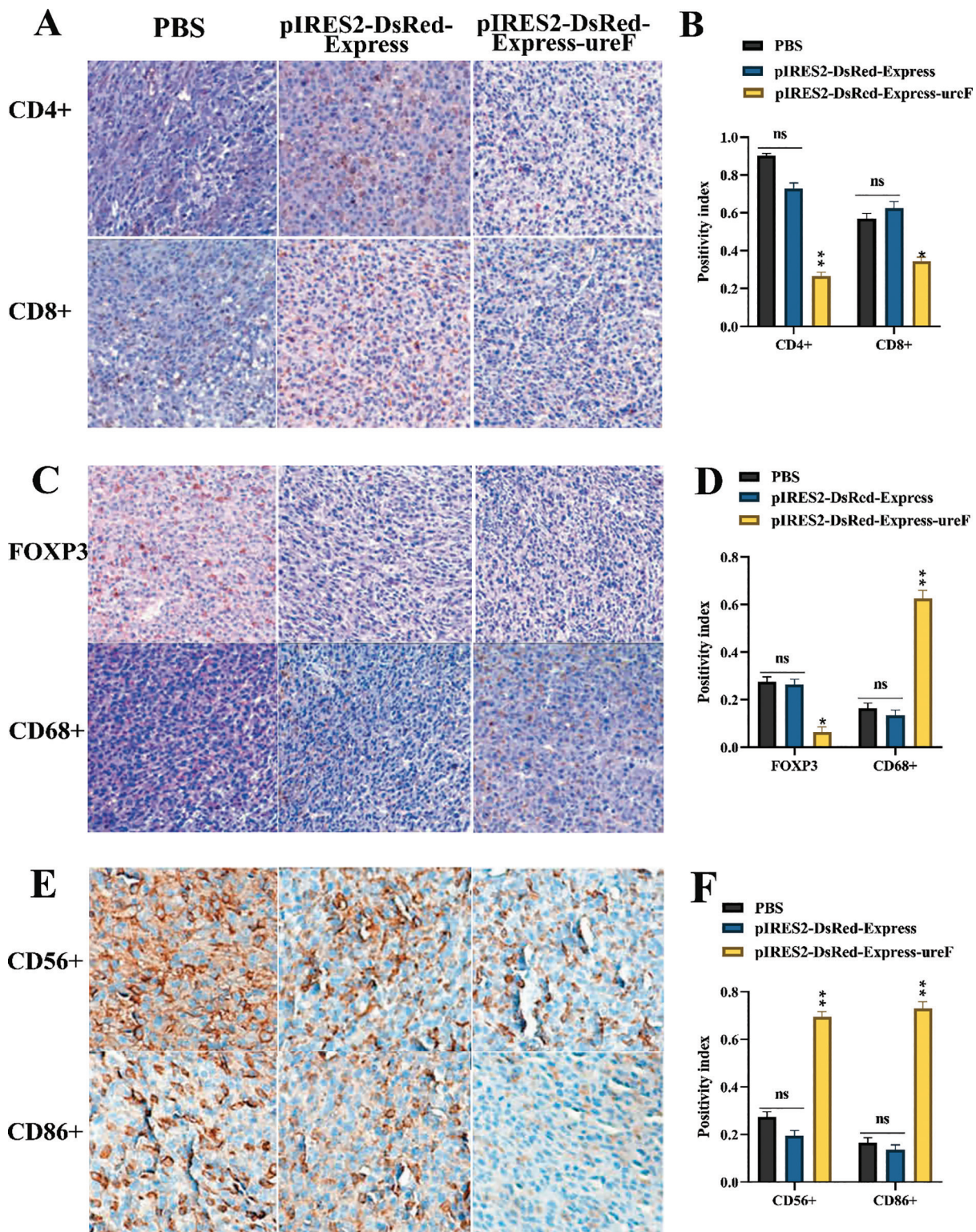


**Fig 6.** Evaluation of the xenograft tumor's infiltrating immune cell subpopulations following adoptive T-cell infusions. (A) Illustration of CD4<sup>+</sup> and CD8<sup>+</sup> T cell invasion using representative staining, 20X magnification. (B) Positive T cell infiltration index and CD8<sup>+</sup>/CD4<sup>+</sup> ratios in different groups. (C) Representative stains showing infiltrating CD68<sup>+</sup> macrophages and FOXP3<sup>+</sup> T cells, 20x magnification. (D) The FOXP3<sup>+</sup> T cell and penetrated CD68<sup>+</sup> macrophage infiltration positivity index. (E) Representative staining of the CD56<sup>+</sup> NK lymphocytes and CD86<sup>+</sup> M1 macrophages invaded, 20x magnification. (F) Positive infiltration index for CD56<sup>+</sup> NK cells and CD86<sup>+</sup> M1 macrophages. \**P*<0.05, \*\**P*<0.01, and ns: not significant.



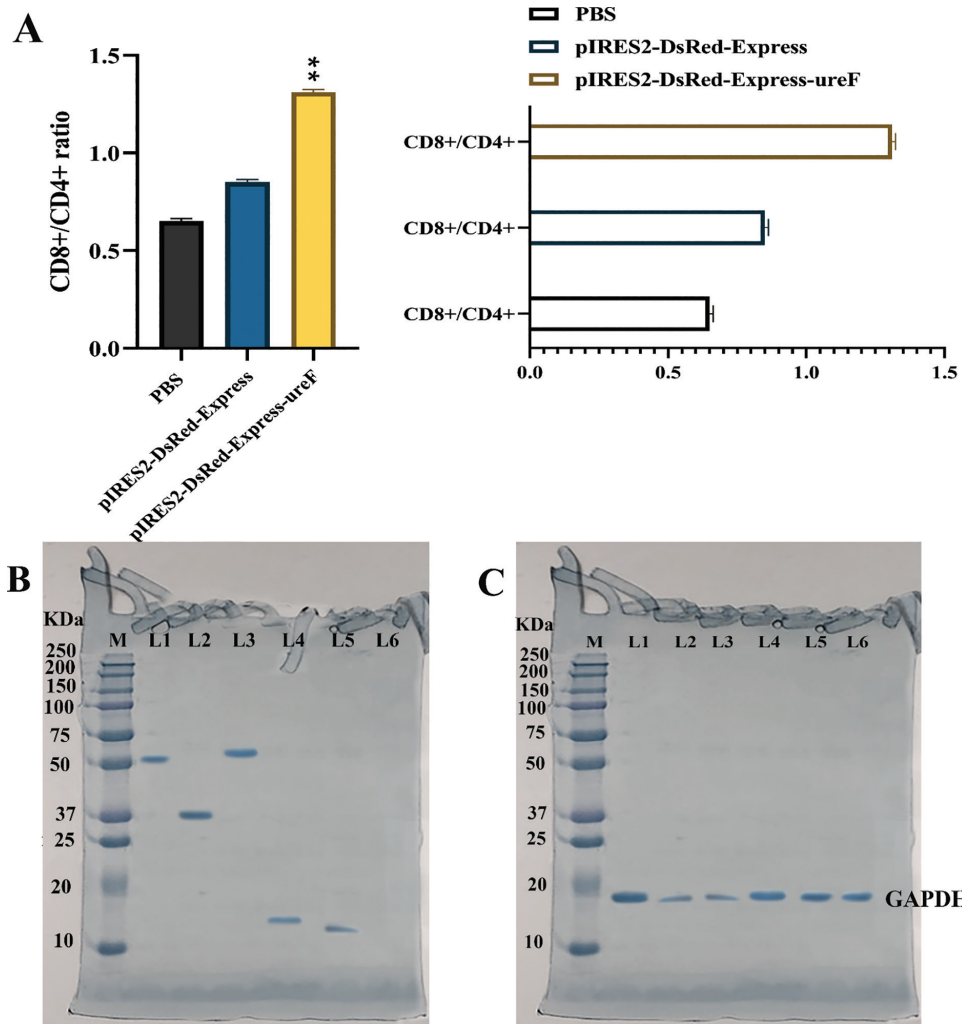


**Fig 7.** (A) Illustration of CD4<sup>+</sup> and CD8<sup>+</sup> T cell invasion using representative staining, 20X magnification. (B) Caspase-9, Caspase-8, Cleaved Caspase-3, and Survivin signals in the xenograft tumor following adoptive T-cell infusions were examined by Western blot analysis. L1: Procaspase-9 (51 kDa); L2: Cleaved Caspase-9 (37 kDa); L3: Caspase-8 (57 kDa); L4: Cleaved Caspase-3 (17 kDa); L5: Survivin (16 kDa); L6: Negative control; M: Protein ladder. (C) L1-L6: GAPDH (20 kDa). \* $P < 0.05$ , \*\* $P < 0.01$ , and ns, not significant.

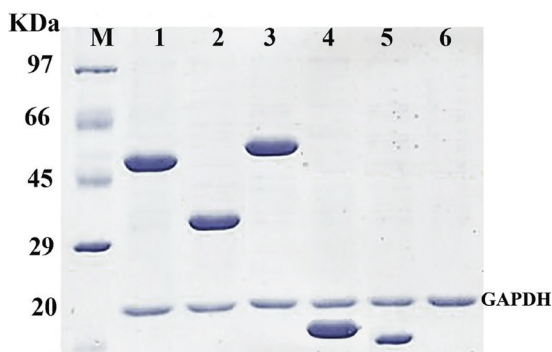


**Fig 8.** Caspase-9, Caspase-8, Cleaved Caspase-3, and Survivin signals in the xenograft tumor following adoptive T-cell infusions were examined by Western blot analysis. 1: Procaspase-9 (51 kDa); 2: Cleaved Caspase-9 (37 kDa); 3: Caspase-8 (57 kDa); 4: Cleaved Caspase-3 (17 kDa); 5: Survivin (16 kDa); 6: Negative control; M: Protein ladder. GAPDH (20 kDa).

## 4. Discussion

Clinical studies demonstrate that regardless of whether they have surgery, GC individuals with positive *H. pylori* infection tend to fare better than those with harmful *H. pylori* infection. After the microorganisms have first caused carcinogenesis, the *H. pylori*-induced immune reaction and chronic infection state may positively influence the development and prognosis of GC (Choi et al. 2012; Xue et al. 2019). This study aims to confirm this notion and investigate any related molecular pathways. Previous research using univariate analysis found a link between seronegative *H. pylori* status and poor outcomes in GC patients (Lee et al. 1995). In addition, two significant prospective studies (Meimarakis et al. 2006; Marrelli et al. 2009) demonstrated the predictive value of positive *H. pylori* status for prolonged relapse-free surviving (RFS) and



overall surviving (OS) in curatively excised GC. These studies show that the median RFS and OS for patients with *H. pylori*-GC are 57 months and 62 months, respectively, as opposed to 19 months and 20 months for patients without *H. pylori*-GC. Patients with *H. pylori*-GC and those without it had 5-year survival rates of 57.0% and 24.0%, respectively (Meimarakis et al. 2006; Marrelli et al. 2009). Some retrospective investigations support the importance of the presence of *H. pylori* as a helpful predictive factor, whereas others do not (Li et al. 2013; Kolb et al. 2017).

The pooled relative risk for OS in patient populations with *H. pylori*-GC compared to those with non-*H. pylori*-GC is 0.71 (95% CI: 0.57–0.87;  $P = 0.001$ ), as demonstrated by the meta-analysis of 12 studies involving 2454 sick people. This finding suggests that *H. pylori* infection plays a defensive function in the prognosis of GC (Wang et al. 2013). Additionally, in the later stages, individuals with *H. pylori*-GC had longer median OS and a more significant response to chemotherapy than patients without *H. pylori*-GC (Choi et al. 2012).

The causes of the disparate outcomes between *H. pylori*-GC and non-*H. pylori*-GC individuals are yet unknown. Some researchers have hypothesized that the increased microsatellite instability brought on by *H. pylori* infection may enhance the prognosis of GC (Kim et al. 2016; Piri-Gharaghie et al. 2022c). Additionally, *H. pylori* infection has been shown to inhibit constitutive production of the monocyte migration inhibitory factor, a possible risk factor for poor survival rates and advanced tumor phases in GC (He et al. 2015). Anti-urease antibodies may facilitate the death and even limit the spreading of cancerous cells in an autoimmune response because urease mimics and binds to specific ligands or surface proteins on gastric epithelial cells and platelets (Scopel-Guerra et al. 2017). Along with increasing the ability to promote antigen processing and presentation, T-cell stimulation and proliferation, and improved antitumor reaction, *H. pylori* infection stimulates monocytes, macrophages, and dendritic cells. Furthermore, it has been suggested that *H. pylori*-GC may boost the anticancer immune reaction (Larussa et al. 2015). Here, DNA vaccines targeting the primary virulence genes (*ureF*) of *H. pylori* are developed and utilized to immunize mice against *H. pylori*-GC. To guarantee good imitation, many techniques are used (Piri-Gharaghie et al. 2022a, 2022b). First, DNA vaccines containing the *ureF* gene are introduced into a vector to prevent product toxicity. Second, to assess the kind and potency of the immune response brought on by the *H. pylori* vaccines, both the IgG subclasses and the Th1 and Th2 reactions are dynamically assessed after vaccination. *ureF* is only one of several *H. pylori* virulence factors that might cause the development of related antibodies. However, compared to the humoral immune reaction by B cells, the T-cell response often has a more significant anticancer effect. Since *H. pylori* infection is most directly related to the development of GC, the splenic CD3<sup>+</sup> T cells generated by DNA

vaccines are categorized and employed for adoptive transfusion to simulate that immunological condition.

A Th1-type response is often induced by acute *H. pylori* infection. It is primarily responsible for the increased release of IFN- $\gamma$ , which causes severe inflammation and cellular damage in the stomach. Despite some contradicting results on the allegedly protective effect of the Th1 reaction, the Th2 response suppresses gastritis generated by pro-inflammatory cytokines and regulates *H. pylori* infection, showing the favorable involvement of the Th2 response in avoiding *H. pylori*-related illnesses (Wang et al. 2007; Xue et al. 2019). Although polarization from the Th1 to Th2 responses has a more significant role during chronic infection, carcinogenesis, and the development of *H. pylori*-GC, the Th1-biased immune reaction is known to be produced early by *H. pylori* infection. Previous identification in *H. pylori*-GC patients supports the growth tendency of IL-4 and IL-10 secretion and the lowering trend of the IgG1/IgG2a proportion (Wang et al. 2007; Xue et al. 2019).

As a result, DNA vaccination causes a switch from Th1 to Th2 responses, which closely resembles the host's shifting immunological state in GC with persistent *H. pylori* infection. In order to imitate the changes in TNF expression brought on by *H. pylori* infection in patients with chronic gastroenteritis, intestinal metaplasia, dysplasia, and GC, the raised TNF level is seen following vaccination (Martínez-Becerra et al. 2012; Ghajari et al. 2021). Additionally, *H. pylori* DNA vaccines cause regional CD3<sup>+</sup>CD4<sup>+</sup> and CD3<sup>+</sup>CD8<sup>+</sup> T lymphocytes to proliferate significantly in mice. This increased proliferation and the effector functions of stimulated CD3<sup>+</sup> T cells likely reduce tumor development and improve the prognosis for *H. pylori*-GC. In a mouse model with tumors, the vaccine-activated splenic CD3<sup>+</sup> T cells are separated, co-cultured with GC cell lines, and given adoptive transfusions. The mean tumor inhibition percentages are 35.8–72.3% *in vivo* and 77.6–4.7% *in vitro*, confirming the anticancer activity of the *H. pylori* pIRES2-DsRed-Express-*ureF* vaccine.

Several pathways have been proposed to explain the anti-GC functions of CD3<sup>+</sup> T lymphocytes generated by *H. pylori* vaccinations. Investigations have been made on the modifications in the immune response of the infiltrating T-cell subpopulations (van den Engel et al. 2006; Xue et al. 2019). In this research, adoptive T-cell transfusions resulted in a considerable reduction in the infiltration of CD4<sup>+</sup> T cells while leaving little to no change in the infiltration of CD8<sup>+</sup> T cells, CD56<sup>+</sup> NK cells, CD68<sup>+</sup> monocytes, or CD86<sup>+</sup> M1 macrophages. Accordingly, the proportions of the infiltrating CD8<sup>+</sup>/CD4<sup>+</sup> T cells rise, indicating that CD8<sup>+</sup> T-cell-dominated polarization is generated and that the particular antitumor actions help improve prognosis. The identification and interaction between antigens and T cell ligands also play a crucial role in T cells' proliferation and anticancer actions (TCRs).

Therefore, it may be assumed that the previously described cross-reaction among GC and *H. pylori* proteins exists. Enhanced cancer cell death by the homed-activated lymphocytes may potentially be caused by an autoimmune pathway, although further research is required to confirm this (Baldari et al. 2005; Xue et al. 2019). The FOXP3<sup>+</sup> Treg cells, which can block a range of immunological responses, are crucial intermediaries of tumor cell tolerance (Shen et al. 2010).

Since adoptive immunotherapy reduces the percentages of FOXP3<sup>+</sup> T cells in this research, transfusion of CD3<sup>+</sup> T cells triggered by the *H. pylori* vaccinations likely lowers the growth or infiltration of Treg cells and, consequently, the Treg-induced immunological tolerance as well (Zhang et al. 2014). Additionally, apoptosis is encouraged following CD3<sup>+</sup> T-cell transfusion, probably due to an increase in Caspase-9/ Caspase3 and a decrease in Survivin, two factors strongly related to the development, infiltration, and migration of GC (Li et al. 2017).

## 5. Conclusion

The DNA vaccines presented here differ from most previously reported vaccinations used to prevent infection since they are deliberately designed to imitate the immunological status generated by chronic *H. pylori* infection. This is done to overcome the limitations. Although they may not provide the highest immunological response, our vaccines and combination vaccination techniques are explicitly developed for this reason. To study how the *H. pylori*-induced T cell reactions affect the development of GC, activated CD3<sup>+</sup> T cells are infused into GC-bearing mice models. It is not comparable to the more challenging condition of a naturally occurring *H. pylori*-GC. Therefore, further research is required to examine the host as well as the immunogens of *H. pylori*. To confirm the molecular basis of the particular anticancer actions of activated T cells, it is first necessary to identify the *TCR* gene spectrum of lymphocytes infiltrated by tumors and compare it

to the epitope patterns of *H. pylori* proteins. In order to rebuild and clarify the natural impacts of the *H. pylori*-related immune function on the prognosis of GC, a conventional mouse model with primary *H. pylori*-GC should be produced, although with challenges.

## Acknowledgments

The authors would like to thank the staff members of the Biotechnology Research Center of the Islamic Azad University of Shahrekord Branch in Iran for their help and support. This research did not receive any specific grant from funding agencies in the public, commercial, or not-for-profit sectors.

## Funding

This research did not receive any specific grant from funding agencies in the public, commercial, or not-for-profit sectors.

## Ethics Approval and Consent to Participate

The study was approved by the Ethics Committee of the Islamic Azad University of Shahrekord Branch in Iran.

## Declaration of Competing Interest

The authors declare that they have no known competing financial interests or personal relationships that could have appeared to influence the work reported in this paper.

## Availability of Data and Material

The datasets analyzed during the current study are available from the corresponding author upon reasonable request.

## References

- Baldari CT, Lanzavecchia A, Telford JL (2005) Immune subversion by *Helicobacter pylori*. Trends Immunol 26:199–207. <https://doi.org/10.1016/j.it.2005.01.007>
- Chehelgerdi M, Doosti A (2020) Effect of the cagW-based gene vaccine on the immunologic properties of BALB/c mouse: An efficient candidate for *Helicobacter pylori* DNA vaccine. J Nanobiotechnol 18:63. <https://doi.org/10.1186/s12951-020-00618-1>
- Choi IK, Sung HJ, Lee JH et al (2012) The relationship between *Helicobacter pylori* infection and the effects of chemotherapy in patients with advanced or metastatic gastric cancer. Cancer Chemother Pharmacol 70:555–558. <https://doi.org/10.1007/s00280-012-1944-5>
- Fakharian F, Asgari B, Nabavi-Rad A et al (2022) The interplay between *Helicobacter pylori* and the gut microbiota: An emerging driver influencing the immune system homeostasis and gastric carcinogenesis. Front Cell Infect Microbiol 12:953718. <https://doi.org/10.3389/fcimb.2022.953718>
- Ghajari G, Nabiuni M, Amini E (2021) The association between testicular toxicity induced by Li2Co3 and protective effect of Ganoderma lucidum: Alteration of Bax & c-Kit genes expression. Tissue Cell 72:101552. <https://doi.org/10.1016/j.tice.2021.101552>

- Gupta N, Maurya S, Verma H et al (2019) Unraveling the factors and mechanism involved in persistence: Host-pathogen interactions in *Helicobacter pylori*. J Cell Biochem 120:18572–18587. <https://doi.org/10.1002/jcb.29201>
- He LJ, Xie D, Hu PJ et al (2015) Macrophage migration inhibitory factor as a potential prognostic factor in gastric cancer. World J Gastroenterol 21:9916–9926. <https://doi.org/10.3748/wjg.v21.i34.9916>
- Kafarski P, Talma M (2018) Recent advances in design of new urease inhibitors: A review. J Adv Res 13:101–112. <https://doi.org/10.1016/j.jare.2018.01.007>
- Kang SY, Han JH, Ahn MS et al (2012) *Helicobacter pylori* infection as an independent prognostic factor for locally advanced gastric cancer patients treated with adjuvant chemotherapy after curative resection. Int J Cancer 130:948–958. <https://doi.org/10.1002/ijc.26081>
- Kim HJ, Kim N, Yoon H et al (2016) Comparison between resectable *Helicobacter pylori*-negative and-positive gastric cancers. Gut Liver 10:212–219. <https://doi.org/10.5009/gnl14416>
- Kolb JM, Ozbek U, Harpaz N (2017) Effect of *Helicobacter pylori* infection on outcomes in resected gastric and gastroesophageal junction cancer. J Gastrointest Oncol 8:583–588. <https://doi.org/10.21037/jgo.2017.01.22>
- Kusters JG, Van Vliet AH, Kuipers EJ et al (2006) Pathogenesis of *Helicobacter pylori* infection. Clin Microbiol Rev 19:449–490. <https://doi.org/10.1128/CMR.00054-05>
- Larussa T, Leone I, Suraci E et al (2015) *Helicobacter pylori* and T helper cells: Mechanisms of immune escape and tolerance. J Immunol Res 2015:981328. <https://doi.org/10.1155/2015/981328>
- Lee WJ, Lin JT, Shun CT et al (1995) Comparison between resectable gastric adenocarcinomas seropositive and seronegative for *Helicobacter pylori*. Br J Surg 82:802–805. <https://doi.org/10.1002/bjs.1800820627>
- Li G, Wang Z, Wang Z et al (2013) Gastric cancer patients with *Helicobacter pylori* infection have a poor prognosis. J Surg Oncol 108:421–426. <https://doi.org/10.1002/jso.23417>
- Li P, Zhou L, Zhao T et al (2017) Caspase-9: Structure, mechanisms and clinical application. Oncotarget 8:23996–24008. <https://doi.org/10.18632/oncotarget.15098>
- Maleki Kakelar H, Barzegari A, Dehghani J et al (2019) Pathogenicity of *Helicobacter pylori* in cancer development and impacts of vaccination. Gastric Cancer 22:23–36. <https://doi.org/10.1007/s10120-018-0867-1>
- Malfertheiner P, Megraud F, Rokkas T et al (2022) Management of *Helicobacter pylori* infection: The Maastricht VI/Florence consensus report. Gut 71:1724–1762. <https://doi.org/10.1136/gutjnl-2022-327745>
- Marrelli D, Pedrazzani C, Berardi A et al (2009) Negative *Helicobacter pylori* status is associated with poor prognosis in patients with gastric cancer. Cancer 115:2071–2080. <https://doi.org/10.1002/cncr.24253>
- Martínez-Becerra F, Castillo-Rojas G, de León SP et al (2012) IgG subclasses against *Helicobacter pylori* isolates: An important tool for disease characterization. Scand J Immunol 76:26–32. <https://doi.org/10.1111/j.1365-3083.2012.02699.x>
- Meimarakis G, Winter H, Assmann I et al (2006) *Helicobacter pylori* as a prognostic indicator after curative resection of gastric carcinoma: A prospective study. Lancet Oncol 7:211–222. [https://doi.org/10.1016/S1470-2045\(06\)70586-1](https://doi.org/10.1016/S1470-2045(06)70586-1)
- Mezmaile L, Coelho LG, Bordin D et al (2020) Review: Epidemiology of *Helicobacter pylori*. Helicobacter 25 Suppl 1:e12734. <https://doi.org/10.1111/hel.12734>
- Nagaraja V, Eslick GD (2014) Evidence-based assessment of proton-pump inhibitors in *Helicobacter pylori* eradication: A systematic review. World J Gastroenterol 20:14527–14536. <https://doi.org/10.3748/wjg.v20.i40.14527>
- O'Connor A, Furuta T, Gisbert JP et al (2020) Review – treatment of *Helicobacter pylori* infection 2020. Helicobacter 25 Suppl 1:e12743. <https://doi.org/10.1111/hel.12743>
- Park HE, Park S, Nizamutdinov D et al (2022) Antigenic determinant of *Helicobacter pylori* FlaA for developing serological diagnostic methods in children. Pathogens 11:1544. <https://doi.org/10.3390/pathogens11121544>
- Piri-Gharaghie T, Doosti A, Mirzaei SA (2022a) Fabrication and characterization of pcDNA3. 1 (+) location within chitosan/nanoparticles complexes for enhanced gene delivery. Iran J Biotechnol 20:e3110. <https://doi.org/10.30498/ijb.2022.297534.3110>
- Piri-Gharaghie T, Doosti A, Mirzaei SA (2022b) Identification of antigenic properties of acinetobacter baumannii proteins as novel putative vaccine candidates using reverse vaccinology approach. Appl Biochem Biotechnol 194:4892–4914. <https://doi.org/10.1007/s12010-022-03995-5>
- Piri-Gharaghie T, Jegargoshe-Shirin N, Saremi-Nouri S et al (2022c) Effects of Imipenem-containing Niosome nanoparticles against high prevalence methicillin-resistant Staphylococcus Epidermidis biofilm formed. Sci Rep 12:5140. <https://doi.org/10.1038/s41598-022-09195-9>
- Ranjbar R, Chehelgerdi M (2018) Genotyping and antibiotic resistance properties of *Helicobacter pylori* strains isolated from human and animal gastric biopsies. Infection and drug resistance. Infect Drug Resist 11:2545–2554. <https://doi.org/10.2147/IDR.S187885>
- Scopel-Guerra A, Olivera-Severo D, Staniscuaski F et al (2017) The impact of *Helicobacter pylori* urease upon platelets and consequent contributions to inflammation. Front Microbiol 8:2447. <https://doi.org/10.3389/fmicb.2017.02447>
- Sharndama HC, Mba IE (2022) *Helicobacter pylori*: An up-to-date overview on the virulence and pathogenesis mechanisms. Braz J Microbiol 53:33–50. <https://doi.org/10.1007/s42770-021-00675-0>
- Shatila M, Thomas AS (2022) Current and future perspectives in the diagnosis and management of *Helicobacter pylori* infection. J Clin Med 11:5086. <https://doi.org/10.3390/jcm11175086>
- Shen Z, Zhou S, Wang Y et al (2010) Higher intratumoral infiltrated Foxp3<sup>+</sup> Treg numbers and Foxp3<sup>+</sup>/CD8<sup>+</sup> ratio are associated

- with adverse prognosis in resectable gastric cancer. *J Cancer Res Clin Oncol* 136:1585–1595. <https://doi.org/10.1007/s00432-010-0816-9>
- Tempera PJ, Michael M, Tageldin O et al (2022) Gastric cancer due to chronic *H. pylori* infection: What we know and where we are going. *Diseases* 10:57. <https://doi.org/10.3390/diseases10030057>
- Tilahun M, Gedefie A, Belayhun C et al (2022) *Helicobacter pylori* pathogenicity Islands and Giardia lamblia cysteine proteases in role of coinfection and pathogenesis. *Infect Drug Resist* 15:21. <https://doi.org/10.2147/IDR.S346705>
- van den Engel NK, Winter H, Rüttinger D et al (2006) Characterization of immune responses in gastric cancer patients: A possible impact of *H. pylori* to polarize a tumor-specific type 1 response? *Clin Immunol* 120:285–296. <https://doi.org/10.1016/j.clim.2006.04.566>
- Wang F, Sun G, Zou Y et al (2013) Protective role of *Helicobacter pylori* infection in prognosis of gastric cancer: Evidence from 2454 patients with gastric cancer. *PLoS One* 8:e62440. <https://doi.org/10.1371/journal.pone.0062440>
- Wang SK, Zhu HF, He BS et al (2007) CagA<sup>+</sup> *H. pylori* infection is associated with polarization of T helper cell immune responses in gastric carcinogenesis. *World J Gastroenterol* 13:2923. <https://doi.org/10.3748/wjg.v13.i21.2923>
- Xue LJ, Mao XB, Liu XB et al (2019) Activation of CD3<sup>+</sup> T cells by *Helicobacter pylori* DNA vaccines in potential immunotherapy of gastric carcinoma. *Cancer Biol Ther* 20:866–876. <https://doi.org/10.1080/15384047.2019.1579957>
- Zhang J, Zhu Z, Sun Z et al (2014) Survivin gene expression increases gastric cancer cell lymphatic metastasis by upregulating vascular endothelial growth factor-C expression levels. *Mol Med Rep* 9:600–606. <https://doi.org/10.3892/mmr.2013.1858>
- Zhang L, Chen X, Ren B et al (2022) *Helicobacter pylori* in the oral cavity: Current evidence and potential survival strategies. *Int J Mol Sci* 23:13646. <https://doi.org/10.3390/ijms232113646>



## Supplementary Material

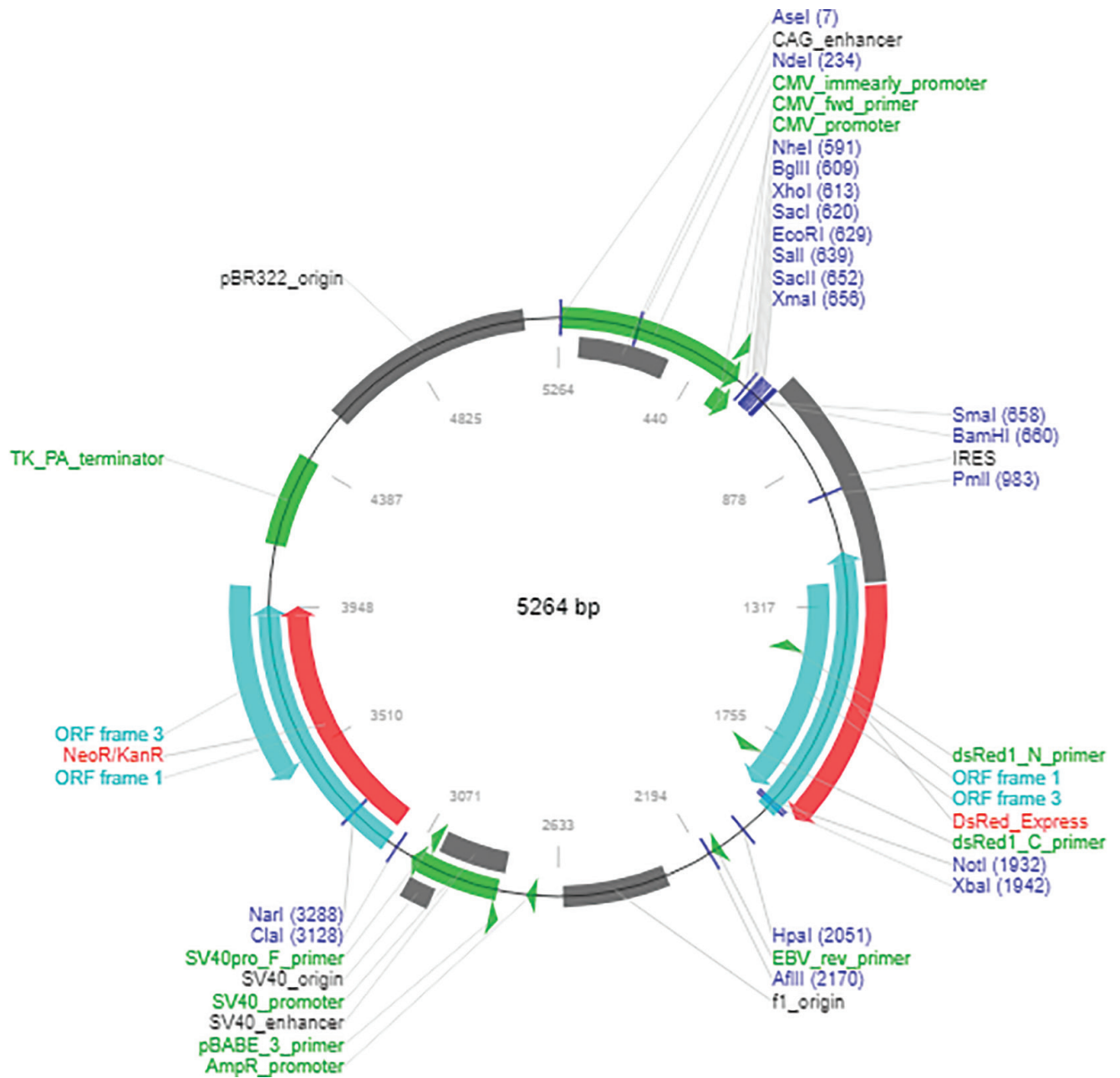


**Fig S1.** Schematic illustration of pIRES2-DsRed-Express plasmid.

TAGCGGTTTG ACTCACGGGG ATTTCCAAGT CTCCACCCCA TTGACGTCAA  
TGGGAGTTTG TTTTGGCACC AAAATCAACG GGACTTTCCA AAATGTCGTA  
ACAACTCCGC CCCATTGACG CAAATGGGCG GTAGGCGTGT ACGGTGGGAG  
GTCTATATAA GCAGAGCTGG TTTAGTGAAC CGTCAGATCC GCTAGCGCTA  
CCGGACTCAG ATCTCGAGGA AAAATAACAG AATGGATAAA GGAAAAAGCG  
TGAAAAGCAC TGAAAAAAGC GTGGGTATGC CCCCAAAAAC CCCAAAGACA  
GACAATAATG TCAATAGTCA TGTAGATAAT GAATTTCTGA TCTTGCAAGT  
CAATGATGCG GTGTTCCCCA TTGGATCTTA CACACATTCT TTTGGGCTAG  
AAACTTATAT CCAGCAAAAA AAGGTTAGCA ATAAAGAAAG CGCTTTAGAG  
TATTTAAAAG CCAATCTTTC TAGCCAGTTC CTTTACACGG AAATGCTGAG  
CTTGAAATTA ACCTATGAAA GCACCCTCCA ACAAGATTTA AAAAAAATCT  
TAGGGGTTGA AGAAATGGTT AGGCTATCCA CAAGCCCCAT GGAATTACGA  
TTAGCCAATC AAAAGCTAGG CAATCGTTTC ATTAACACCT TACAAGCCAT  
GAACGAATTA GACATGGGTG CATTTTTTAA CGTTACGCT CAACAAACCA  
AAGATCCAC CCATGCCACT AGCTATGGCG TTTTTCGGC GAGTTTGAAT  
ATGGAATTGA AAAAGGCTTT AAGGCATTAT CTTTATGCAC AACTTCTAA  
CATGGTGATC AACTGCGTTA AAAGCGTCCC ACTATCTCAA AACGACGGGC  
AAAAAATCTT ATTGAGCTTG CAAAGCCCTT TTAACCAGCT CATAGAAAAA  
ACCCTAGAAC TAGACGAAAG CCACCTATGC GCGGCAAGCG TTCAAACGA  
CATTAAAGCG ATGCAGCATG AGAGTTTATA CTCGCGCCTT TATATGTCTT  
GAATTTTAGA GCTCAAGCTT CGAATTCTGC AGTCGACGGT ACCGCGGGCC  
CGGGATCCGC CCCTCTCCCT CCCCCCCCCC TAACGTTACT GGCCGAAGCC  
GCTTGGAATA AGGCCGGTGT GCGTTTGTCT ATATGTTATT TTCCACCATA  
TTGCCGTCTT TTGGCAATGT GAGGGCCCCG AACCTGGCC CTGTCTTCTT  
GACGAGCATT CCTAGGGGTC TTTCCCCTCT CGCCAAAGGA ATGCAAGGTC  
TGTTGAATGT CGTGAAGGAA GCAGTTCCTC TGGAAGCTTC TTGAAGACAA  
ACAACGTCTG TAGCGACCCT TTGCAGGCAG CGGAACCCCC CACCTGGCGA

**Fig S2.** DNA sequence of ureF target gene inserted into pIRES2-DsRed-Express vector.

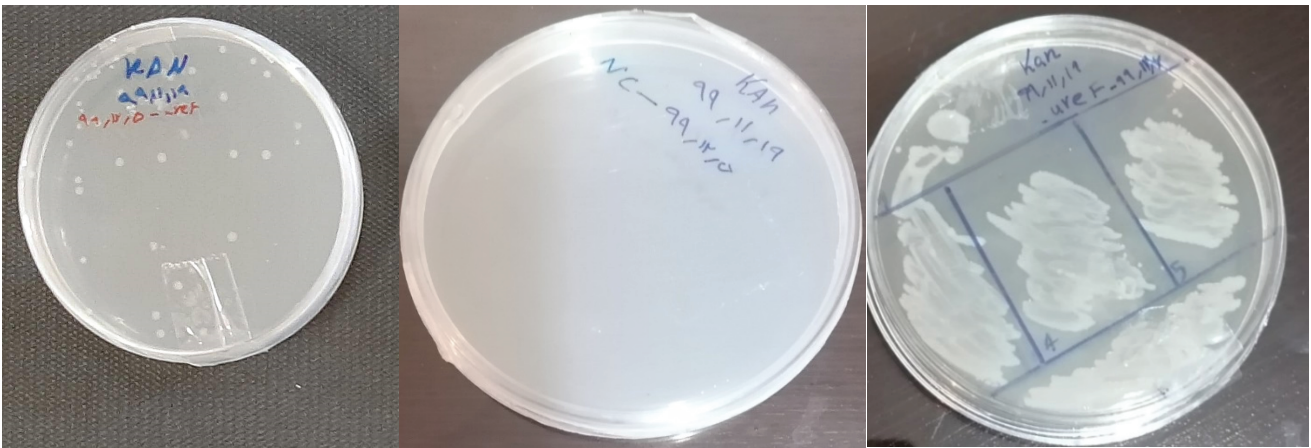


**Fig S3.** Single colonies of transformed bacteria containing plasmid with *ureF* gene; Non-growth of vector-free cells in agar medium containing the antibiotic kanamycin (negative control); Preparation of matrix from a number of selected colonies.

**Table S1.** The number of mice used in this experiment

Group number	Injection composition	Number of mice	Average weight of mice	Type of injection	Time of injection (Day)
1	pIRES2-DsRed-Express- <i>ureF</i>	20	19.7 ± 0.5	IM	0, 15, 30
2	pIRES2-DsRed-Express	20	18.2 ± 0.7	IM	0, 15, 30
3	PBS	20	19.4 ± 0.68	IM	0, 15, 30